PbS-Doped Mesostructured Silica Films with High Optical Nonlinearity

Dario Buso, Paolo Falcaro, Stefano Costacurta, Massimo Guglielmi, and Alessandro Martucci*

INSTM—Dipartimento di Ingegneria Meccanica, Settore Materiali, Università di Padova, Via Marzolo 9, 35131 Padova, Italy

Plinio Innocenzi and Luca Malfatti

Dipartimento di Architettura e Pianificazione, Università di Sassari, Nanoworld Institute, Palazzo Pou Salit, Piazza Duomo 6, 07041 Alghero Sassari, Italy

Valentina Bello, Giovanni Mattei, and Cinzia Sada

INFM—Dipartimento di Fisica "Galileo Galilei", Università di Padova, via Marzolo 8, 35131 Padova, Italy

Heinz Amenitsch

Institute of Biophysics and X-ray Structure Research, Austrian Academy of Sciences, Schmiedelstrasse, A-8042, Graz, Austria

Irina Gerdova and Alain Haché

Département de Physique et d'Astronomie, Université de Moncton, Moncton, Canada

Received April 21, 2005. Revised Manuscript Received August 1, 2005

Mesostructured silica films have been doped with lead sulfide (PbS) nanocrystals by a two-step impregnation, using the mesopores as nanoreactors for PbS growth. Secondary ion mass spectrometry and transmission electron microscopy characterizations demonstrated nanocrystals growth inside the pores and throughout the film thickness, pointing out the feasibility of an impregnation-based synthesis made possible by the porous properties of mesoporous silica films. The mean particles diameter is 5 nm, which is compatible with the pore dimensions. The mesostructure order was retained after the growth of the nanocrystals, as pointed out by small-angle X-ray scattering measurements. Optical absorption and *Z*-scan measurements indicated that PbS nanoparticles show a quantum confinement effect, while the films are characterized by high nonlinearities of the optical response. The optical properties of this material can be usefully exploited in several nonlinear optical applications.

Introduction

The introduction of nanoparticles inside host matrixes has been intensively studied in the past decade, and several synthetic approaches have been reported. The pores of various mesoporous materials have been filled with semiconductors (CdS, CdSe, GaN, InP),[1,2] metal oxides (Fe_2O_3, Mn_3O_4),[2,3] and metals (Au, Ag, Pt)[4−7] in order to obtain materials with unique chemical, catalytic, magnetic, and optical properties. The techniques range from simple solution process to chemical vapor infiltration.[1,2,6] Also two-step syntheses are reported, using micelle cores of special block copolymers first as growing sites for the particles and then as templates using the micelle cores as porogens.[8] The formation of host−guest composites of different kinds of nanoparticles embedded within the micromesopores has been described mostly for powders.[1−7,9,10] Powders are unfavorable with respect to the potential application in nonlinear optics and in the optical characterization of the composites: intense light scattering induced by a large numbers of individual

* Corresponding author. E-mail: alex.martucci@unipd.it. Fax: +39 049 827 5505.

(1) Wark, M.; Wellmann, H.; Rathousky, J. *Thin Solid Films* **2004**, *458*, 20.
(2) Winkler, H.; Birkner, A.; Hagen, V.; Wolf, I.; Fisher, R. A.; Schmechel, R.; Seggern, H. V. *Adv. Mater.* **1999**, *11*, 1444.
(3) Folch, B.; Larionova, J.; Guari, Y.; Guérin, C.; Mehdi, A.; Reyé, C. *J. Mater. Chem.* **2004**, *14*, 2703.
(4) Liu, Z.; Sakamoto, Y.; Ohsuna, T.; Hiraga, K.; Terasaki, O.; Ko, C. H.; Shin, H. J.; Ryoo, R. *Angew. Chem., Int. Ed.* **2000**, *39*, (17), 3107.
(5) Fukuoka, A.; Araki, H.; Sakamoto, Y.; Inagaki, S.; Fukushima, Y.; Ichikawa, M. *Inorg. Chim. Acta* **2003**, *350*, 371.
(6) Wu, Y.; Zhang, L.; Li, G.; Liang, C.; Huang, X.; Zhang, Y.; Song, G.; Jia, J.; Zhixiang, C. *Mater. Res. Bull.* **2001**, *36*, 253.
(7) Arbiol, J.; Cabot, A.; Morante, J. R.; Chen, F.; Liu, M. *Appl. Phys. Lett.* **2002**, *81*, 3449.
(8) Bronstein, L.; Krämer, E.; Berton, B.; Burger, C.; Förster, S.; Antonietti, M. *Chem. Mater.* **1999**, *11*, 1402.
(9) Wark, M.; Jaeger, N. I.; Lutz, W.; Tkachenko, O. P.; Bunsenges, B. *Phys. Chem.* **1997**, *69*, 1635.
(10) Wellmann, H.; Rathousky, J.; Wark, M.; Zukal, A.; Schulz-Ekloff, G. *Microporous Mesoporous Mater.* **2001**, *44−45*, 419.

10.1021/cm050850j CCC: $30.25
Published on Web 09/08/2005

crystallites hinders the transmission mode, therefore diffuse reflectance techniques must be employed and data modeling is needed.[11] For this work, mesostructured silica films obtained through evaporation-induced self-assembly (EISA)[12] have been used as nanoreactors for in situ growing of lead sulfide nanocrystals by means of impregnation of suitable precursors. The dimensional control of the nanocavities inside the mesostructured silica host allows the tailoring of the shape and dimensional features of the nanoparticles. Nanometric dimensions of the cavities induce the growth of PbS nanocrystals showing quantum size confinement. Due to their predominantly ionic character and low optical band gap (0.41 eV, corresponding to $\lambda = 3200$ nm), PbS nanoparticles show quantum confinement effects up to a larger dimensional range compared to those of other binary semiconductors with predominantly covalent character (such as CdS and ZnS).[13] Together with the high third-order optical nonlinearity observed, this makes the lead sulfide doped silica films described here suitable for optical applications in devices that require small band gap semiconductors, ranging from the visible range to the near-infrared (NIR) spectrum. Furthermore, the high third-order nonlinearity of PbS nanoparticles could be exploited in high-speed optical switching.[14]

Experimental Section

Mesostructured Silica Matrixes. A stock solution was prepared with TEOS, EtOH, and an HCl aqueous solution. The molar ratios were TEOS/EtOH/HCl/H_2O = 1/2.78/1.45 × 10^{-2}/1.17. This solution was stirred for 1 h to allow a slight precondensation of the silane units. Meanwhile, a template solution was prepared by dissolving 1.3 g of Pluronic F127 in 15 mL of EtOH and adding 1.5 mL of HCl 0.005M. Finally, 7.7 mL were taken from the stock solution and added to the template one.

For GI-SAXS, SIMS, and TEM measurements, p-type/boron-doped/(100) oriented silicon substrates were chosen for the film deposition. XRD, UV−vis absorption, and *Z*-scan measurements were carried out on films deposited on glass substrates.

Dip-coating of the solution was performed employing a home-built dip-coating system.[15] The relative humidity (RH%) in the deposition chamber was set at 40%, while the withdrawal speed was set at 15 cm/min. The samples were thermally treated in air, following a ramp consisting of three steps: (1) 150 °C for 20 min, (2) 250 °C for 20 min, and (3) 350 °C for 1 h.

Impregnation with PbS Precursors and Nanoparticle Growth. Two separate solutions were made, containing the lead and the sulfur precursor, respectively. Lead acetate ($Pb(CH_3COO)_2 \cdot 3H_2O$, $PbAc_2$) was dissolved in MeOH in the presence of acetic acid (HAc) to get solution 1, using molar ratios set at MeOH/PbAc/HAc = 1/0.01/0.05. Solution 2 was prepared dissolving thioacetamide (CH_3CSNH_2, TAA) in MeOH according to MeOH/TAA = 1/0.04. The Pb to S molar ratio was set to 1/1.

The mesostructured films were first immersed into solution 1 at room temperature for 24 h to allow the diffusion of the lead precursor solution inside the pores. The films were then removed from solution 1 and carefully washed with pure MeOH to eliminate residual lead acetate solution; this was made to induce the presence of Pb^{2+} cations only in the inner pores of the film and not on its external surface. The film surface was then dried under a dry air flux, and the film was later completely immersed into solution 2; this was kept at 60 °C to optimize the diffusion rate of the sulfur anions through the pore interconnections. The samples were kept in solution 2 for 60 min and finally extracted and washed in pure MeOH. The films looked homogeneously dark-brown immediately after extraction from solution 2, indicating PbS formation.

Material Characterization. The ordered mesostructure of the host silica matrix was investigated using the high-flux grazing incidence small-angle X-ray scattering (GI-SAXS) apparatus at the Austrian high-flux beamline of the electron storage ring ELETTRA (Trieste, Italy).[16] Images of samples (either before or after impregnation) were acquired with exposure times ranging from 200 ms to 24 s. The selected incident radiation energy was 8 keV, corresponding to a wavelength of 1.54 nm. The instrumental grazing angle was set maintaining an incident X-ray beam smaller than 3°. The images were collected by a CCD detector and processed using the "fit2d" program.[17] Before GI-SAXS data analysis, the collected images were corrected with fit2d: the intensity of the images was normalized, the spatial distortion was corrected, and instrumental errors (background noise and dark current) were subtracted.

Secondary ion mass spectrometry (SIMS) measurements were carried out by means of an IMS 4f mass spectrometer (Cameca, Padova, Italy) using a 10 kV Cs^+ primary beam and by negative secondary ion detection (the sample potential was fixed at −4.5 kV) with a final impact energy of 14.5 keV. The SIMS spectra were collected in ultrahigh vacuum conditions at different primary beam intensity (15 nA) rastering over a nominally 125 × 125 μm^2 area. Beam-blanking mode was used to improve the depth resolution, interrupting the sputtering process during magnet stabilization periods. The erosion speed was then evaluated by measuring the depth of the erosion crater at the end of each analysis by means of a Tencor Alpha Step profilometer with a maximum uncertainty of a few nanometers. The measurements were performed in high mass resolution configuration to avoid mass interference artifacts. The charge buildup while profiling the insulating samples was compensated by an electron gun without any need to cover the surface with a metal film.

Structural and compositional characterization was performed by means of transmission electron microscopy (TEM). The measurements were carried out at CNR-IMM (Bologna, Italy) on cross-sectional samples with a field-emission FEI TECNAI F20 SuperTwin FEG-(S)TEM microscope operating at 200 kV. TEM is equipped with an Edax energy-dispersive X-ray spectrometer (EDXS) for compositional analysis and a Gatan 794 multiple scan camera, allowing digital image recording on a 1024 × 1024 pixels CCD array.

The films were characterized after the impregnation process by X-ray diffraction (XRD) using a diffractometer equipped with grazing incidence X-ray optics. The analysis was performed using Cu Kα Ni-filtered radiation at 40 kV and 40 mA. The average crystallite size was calculated using the Scherrer correlation after fitting the experimental profiles with a pseudo-Voigt function.

UV−vis absorption spectra were taken using a Jasco V-570 spectrometer, performing the measurement at room temperature. The measurement was conducted investigating the optical response

(11) Kubelka, P.; Munk, F. *Z. Technol. Phys.* **1931**, *12*, 593.
(12) Brinker, C. J.; Lu, Y.; Sellinger, A.; Fan, H. *Adv. Mater*. **1999**, *11*, 579.
(13) Chakraborty, I.; Moulik, S. P. *J. Nanopart. Res.* **2004**, *6*, 233.
(14) Colvin, V. L.; Schlamp, M. C.; Alivisatos, A. P. *Nature* **1994**, *370*, 354.
(15) Falcaro, P.; Costacurta, S.; Mattei, G.; Amenitsch, H.; Marcelli, A.; Cestelli Guidi, M.; Piccinini, M.; Nucara, A.; Malfatti, L.; Kidchob, T.; Innocenzi, P. *J. Am. Chem. Soc.* **2005**, *127* (11), 3838.
(16) Amenitsch, H.; Rappolt, M.; Kriechbaum, M.; Mio, H.; Laggner, P.; Bernstorff, S. *J. Synchrotron Radiat.* **1998**, *5*, 506.
(17) Hammersley, A. P. *ESRF*; available at http://www.esrf.fr/computing/scientific/FIT2D/.

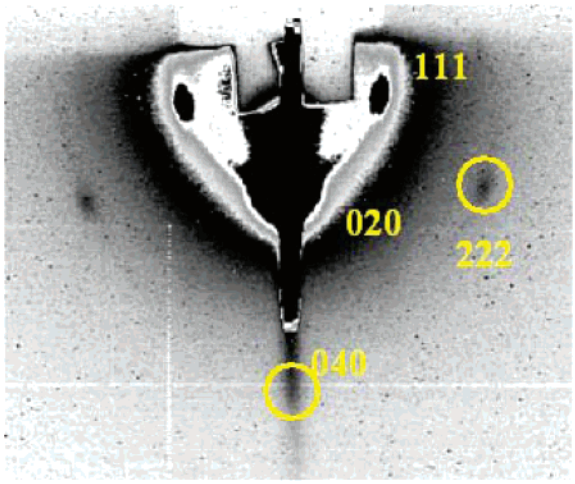

Figure 1. GI-SAX diffraction pattern of the film after impregnation. The evidenced reflections are generated by (111), (020), (222) and (040) planes, consistent with a body-centered tetragonal (BCT) phase (point group *Fmmm*) mesostructure of the silica film.

in the UV, visible, and part of the near-infrared range. The measurement has been conducted using an integrating sphere in order to collect both the direct and the diffused transmission of the samples.

The *Z*-scan experiment was performed using an optical parametric amplifier (OPA 9400, Coherent Inc.) tunable from 460 to 700 nm with 100 kHz repetition rate. The OPA is pumped at 800 nm with a regenerative amplifier seeded by a high-repetition rate Ti:sapphire laser. The duration of the OPA pulses are 260 fs. The spatial profile of the laser beam was near $TEM_{0,0}$ after passing through a spatial filter. A variable-diameter aperture was placed before the calibrated detector, and the beam passing through it was monitored as a function of the position *z* of the sample. The laser pulse energy was controlled by a photodiode. The beam waist in the focal plane was 8 μm. A 10 cm focal length lens was used to focus the beam on the sample, providing an on-axis intensity of up to 10 GW/cm^2. The glass substrate did not give a contribution to the nonlinear properties under the intensities we worked.

Results

Structural Characterization. Figure 1 shows the GI-SAXS image of an impregnated sample, showing a diffraction pattern that can be referred to ordered mesoporous domains. The positions of the defined spots have been used to define the mesostructure following the same procedure described in previous works.[15] The diffraction pattern is in agreement with orthorhombic mesostructured domains. No appreciable microstructural changes were detected comparing SAXS measurements before and after the silica matrix impregnation.

The SIMS plot reported in Figure 2 shows the depth profiling of atomic species detected in the film thickness after impregnation. From bottom to top the straight lines in the depth range of 0−500 nm reveal, respectively, the Pb, S, Si, and O atoms signals. The estimated thickness of the film is 501 ± 27 nm.

Figures 3 and 4 show cross-sectional TEM images of the doped films. The image of Figure 3 shows both the matrix mesostructured domains and some of the PbS nanoparticles that formed inside the pores. The inset of Figure 3 shows a high-resolution TEM (HRTEM) image of a single PbS

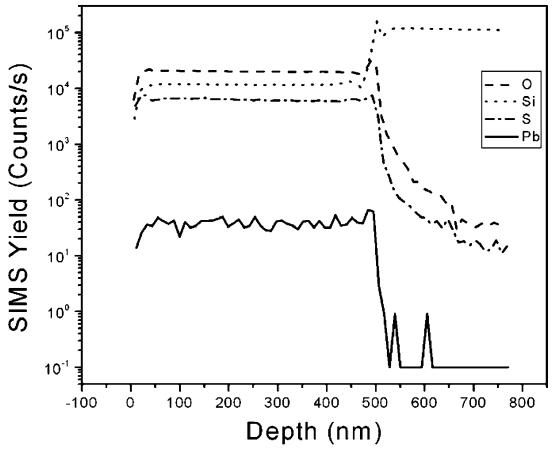

Figure 2. SIMS pattern of the film after impregnation. O, Si, S, and Pb species signals are reported.

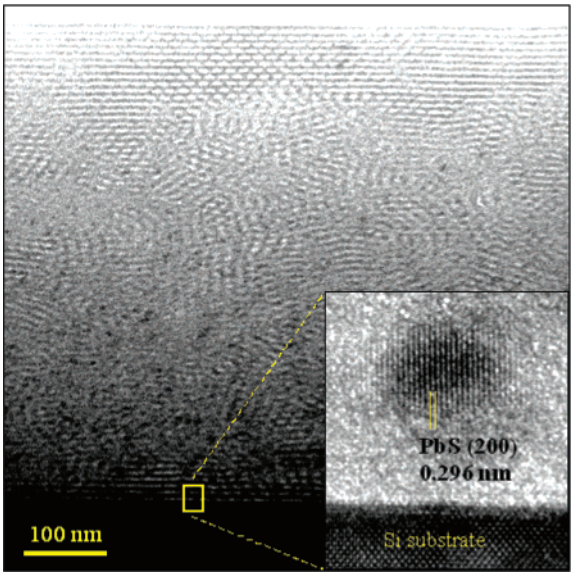

Figure 3. TEM image of the doped film cross section. The scale reported is 100 nm. The inset of the figure reports a HRTEM image of a single PbS nanoparticle formed near the Si−SiO_2 interface. (200) Planes are evidenced together with the lattice distance.

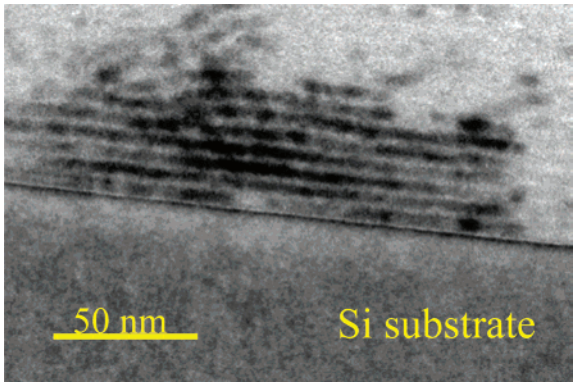

Figure 4. TEM image showing PbS nanoparticles grown inside ordered channels that lie parallel to the film−substrate interface.

nanoparticle that precipitated in a pore near the substrate surface. The atomic structure of (200) plains of the PbS $Fm\bar{3}m$ symmetry (with interplanar distance of 0.296 nm) is clearly visible in the image.

The diffraction pattern of the impregnated film is reported in Figure 5.

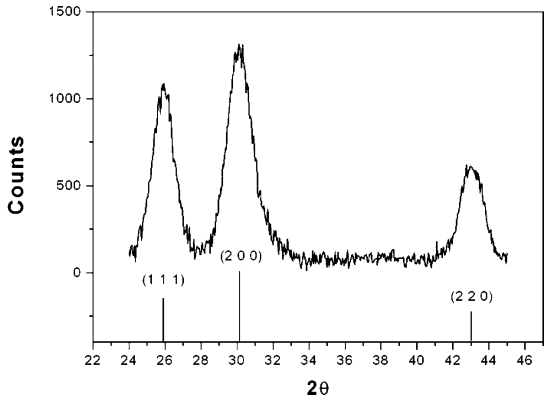

Figure 5. XRD diffraction pattern of the film after impregnation. Peaks generated by (200), (111), and (220) planes belonging to the PbS cubic structure are reported.

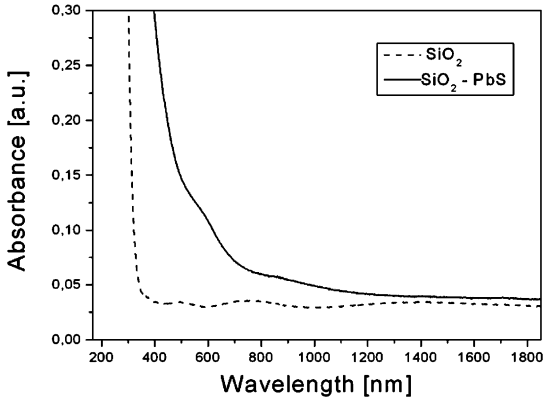

Figure 6. UV−vis−NIR absorption spectra of undoped silica matrix (dotted line) and PbS-doped film (solid line). The films were deposited on soda−lime glass.

Peaks at 25.9°, 30.1°, and 43° show reflections of (111), (200), and (220) planes belonging to crystalline PbS (powder diffraction file No. 05-0592, International Center for Diffraction Data, Newton Square, PA). The crystal size evaluated with Scherrer correlation resulted to be 5 nm.

Optical Characterization. The optical absorbance spectrum of the impregnated film is shown in Figure 6.

The dotted line reports the absorbance of undoped mesostructured silica matrix, while the solid line refers to the PbS-doped one. Interference bands are evident in the whole signal range for the undoped silica film plot (dashed line), while in the case of PbS-doped film the interference effect is limited. The absorption pattern of the doped film has a long tail with no evidence of sharp peaks, and the absorption edge is strongly blue shifted compared to the band gap value of the bulk PbS.

Figures 7 and 8 show the *Z*-scan experimental results and the normalized transmittance measurements in an open-aperture scheme for the investigated film. The nonlinear absorption coefficient varies from $(4.0 \pm 1.0) \times 10^{-7}$ cm/W at 620 nm to $(12.0 \pm 1.0) \times 10^{-7}$ cm/W at 500 nm.

Discussion

The impregnation strategy was chosen after previous considerations on FTIR spectra of the silica matrix, regarding its chemical composition and microstructure. The choice of the thermal treatment was made considering the cross-linking

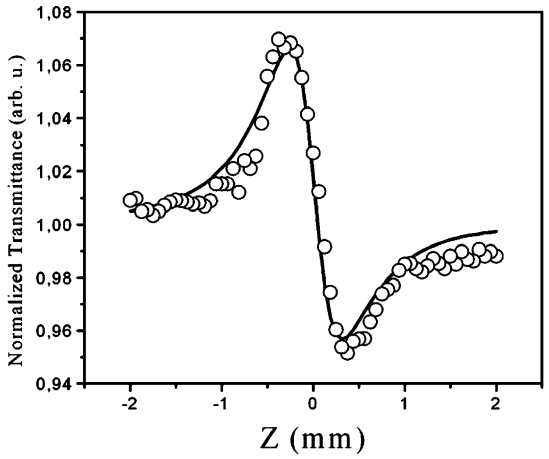

Figure 7. The normalized transmission dependences for the film doped with the PbS quantum dots in the closed-aperture *Z*-scan scheme; $\lambda = 620$ nm, $I_0 = 5.17$ GW/cm^2. The circles are measured data; the solid curves are the theoretical fits described in the text.

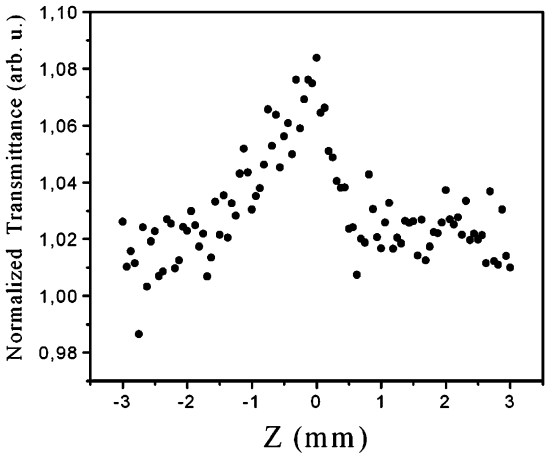

Figure 8. The normalized transmission dependences for the film doped with the PbS quantum dots in the case of the open-aperture *Z*-scan scheme; $\lambda = 620$ nm, $I_0 = 5.17$ GW/cm^2.

extent of the film, which can be evaluated from the position of the Si−O−Si stretching mode at ∼1078 cm^{-1} and from the intensity of the Si−OH vibration mode at 960 cm^{-1}. The correlation between these FTIR data and the SiO_2 cross-linking is explained in a previous work.[18]

The porosity of the mesostructured silica film suggested a first impregnation step with a solution of Pb^{2+} cations and a second impregnation step consisting of the immersion of the Pb^{2+}-impregnated matrix into a solution containing S^{2-} anions. The driving force for the PbS formation is the low solubility of PbS in liquid solutions: the impregnation process provides a supersaturated environment of PbS constituents that leads to PbS crystals precipitation.[19] The procedure was developed considering two competitive processes: the anion diffusion through the interconnected pores and the precipitation of PbS crystals inside the pores. The latter must not hinder the diffusion of the S^{2-} unreacted anions through the whole film thickness. To achieve this aim, the temperature

(18) Falcaro, P.; Grosso, D.; Amenitsch, H.; Innocenzi, P. *J. Phys. Chem. B* **2004**, *108*, 10942.
(19) Privman, V.; Goia, D. V.; Park, J.; Matijević, E. *J. Colloid. Interface Sci.* **1999**, *213*, 36.

of the second step of the impregnation process was set to 60 °C after preliminary trials.

Reflection spots visible in the GI-SAXS spectra of Figure 1 show an orthorhombic mesostructure. Not very many diffraction spots are present even for high exposition times or electrical instrumental amplification, meaning that the film is organized in mesostructured domains mixed with disordered domains. The same conclusion can be derived considering the TEM images that show the whole silica matrix microstructure as an ensemble of submicrometric domains with locally ordered structure. GI-SAXS diffraction pattern (Figure 1) after the PbS nanoparticles growth was not appreciably different from the one obtained from the undoped matrix: the synthesis preserved the original mesostructure without a significant increase of disorder. On the other hand, the nanoparticles do not break the matrix during their growth so that it can be assumed that the pores act as reactors for the nanocrystals formation.

The SIMS measurement is reported in Figure 2. The linearity of the response associated to the lead and sulfur atoms reveals their homogeneous dispersion through the entire silica matrix thickness, this being a proof of the complete penetration of the PbS constituents inside the silica mesostructured film.

The TEM image of Figure 4 clearly shows that PbS particle growth took place inside the mesopores. The inset of Figure 3 shows a HRTEM image that allows us to point out that each nanoparticle is a spheric PbS monocrystal, with an average diameter of 5 nm. Considerations on the nanocrystals growth can be made observing the TEM images and considering that no capping agent was employed in order to tailor the PbS nanoparticles shape and dimensions. PbS nanocrystal growth is first controlled by the surface energy of the nuclei that are forming, and the particles assume spherical shape in order to minimize it. Second, the pore walls prevent them from aggregating into bigger clusters, therefore conditioning their final shape and dimensions.

The inset of Figure 3 shows the image of a single PbS nanoparticle precipitated close to the interface between the film and the silicon substrate. Also, the image in Figure 4 shows PbS particles laying inside pores near the film−substrate interface. Together with the SIMS plot an indirect proof that the pores inside the silica matrix are strictly interconnected is given. The HRTEM image showed that the PbS nanoparticles are monocrystalline.

EDS analysis was performed on several regions of the sample section, pointing out that the Pb to S molar ratio has a value constantly around 1 in all the volumes investigated, as was expected considering the stoichiometric composition of lead sulfide. Furthermore the Pb-to-Si ratio evaluated by EDS analysis performed scanning only the silica film area resulted to be 0.08. Assuming that the Si signal detected is referable unambiguously to the silica SiO_2 matrix (and not to the Si substrate), the molar concentration of PbS inside the film is therefore 8%.

The XRD spectrum (Figure 5) confirms the presence of crystalline lead sulfide, precipitated during the impregnation process. Peaks are consistent with a $Fm\bar{3}m$ face-centered cubic structure. The mean diameter of the PbS nanoparticles evaluated from line broadening of the main diffraction peaks ranged from 4.5 to 6 nm, in good agreement with the average diameter evaluated from the TEM measurements. Furthermore, both particles diameter and pore dimensions[20] are of the same order of magnitude.

The large blue shift of the UV−vis absorption of PbS-doped films (Figure 6) is representative of a quantum confinement effect due to the reduced nanoparticles size. This was expected considering that the PbS particles diameter (5 nm) is smaller than the Bohr radius of the exciton in bulk PbS crystals (18 nm).[13,21]

The exact identification of the absorption edge of the PbS-doped film was made difficult by the absence of resolved subbands. The long tail visible in the whole plot can be due to defects states, wide particle size distribution, and/or indirect transition.[22−24] Estimation of the band gap value of PbS nanoparticles can be made using the empirical correlation reported in the literature,[25] which directly links spherical PbS nanocrystals main diameter to the value of the electronic band gap. The spherical shape of the nanoparticles can be assumed considering the TEM and HRTEM images of a single nanocrystal. The calculated value of the band gap (for 5 nm diameter particles) is 0.933 eV, corresponding to an absorption edge at 1318 nm, in reasonable agreement with the shape of the absorption tail visible in the PbS spectrum of Figure 6.

The interference fringes observed in the undoped films (Figure 6) are caused by the reflection at the film−air and film−substrate interfaces, while in the case of the doped matrix the PbS absorption probably reduces the interference effect.

The sign and magnitude of the third-order nonlinear optical susceptibility of the film doped with PbS quantum dots was measured by a far-field *Z*-scan method. The *Z*-scan technique and its interpretation are described in the literature. In essence, this method extracts the nonlinear refractive index from changes in the phase front and amplitude of a beam propagating in a material. One of the advantages of the *Z*-scan method is the possibility to distinguish two nonlinear optical mechanisms when they are present simultaneously. In the general case, when there is a contribution of both nonlinear refraction and nonlinear absorption or two-photon absorption, the normalized, on-axis transmittance T of a Gaussian input beam as a function of z in the case of closed-aperture *Z*-scan layout is given by the following:[27]

$$T = 1 + 2\Delta\Phi\left[\frac{2\eta}{(1+\eta^2)(9+\eta^2)}\right] - 2\Delta\psi\left[\frac{3+\eta^2}{(1+\eta^2)(9+\eta^2)}\right] \quad (1)$$

where $\eta = z/z_0$, with $z_0 = k\omega_0^2/2$ the diffraction length of

(20) Bearzotti, A.; Mio Bertolo, J.; Innocenzi, P.; Falcaro, P.; Traversa, E. *J. Eur. Ceram. Soc.* **2004**, *24*, 1969.
(21) Xu, L.; Zhang, W.; Ding, Y.; Yu, W.; Xing, J.; Li, F.; Qian, Y. *J. Cryst. Growth* **2004**, *273*, 213.
(22) Borelli, N. F.; Smith, D. W. *J. Non−Cryst. Solids* **1994**, *180*, 25.
(23) Wang, Y.; Suna, A.; Mahler, W.; Kasowsky, R. *J. Chem. Phys.* **1987**, *87*, 7315.
(24) Ricolleau, C.; Gandais, M.; Gacoin, T.; Boilot, J. P. *J. Cryst. Growth* **1996**, *166*, 769.
(25) Kane, R. S.; Cohen, R. E.; Silbey, R. *J. Phys. Chem.* **1996**, *100*, 7928.

the Gaussian beam, $k = 2\pi/\lambda$ is the wavenumber, ω_0 is the radius at the beam waist, and $\Delta\Phi = kn_2I_0L_{\text{eff}}$ and $\Delta\psi = \beta I_0 L_{\text{eff}}/2$ are the phase changes due to nonlinear refraction and nonlinear absorption, respectively. Here, I_0 is the laser beam peak intensity in the focal plane, $L_{\text{eff}} = [1 - \exp(-\alpha_0 L)]/\alpha_0$ is the effective length of the sample, α_0 is the linear absorption coefficient, L is the sample length, n_2 is the nonlinear refractive index, and β is the nonlinear absorption coefficient. The characteristic shape of the *Z*-scan trace reported in Figure 8 indicates a negative refractive nonlinearity. The nonlinearr refractive index (n_2) in this region was measured evaluating the difference in the peak-to-valley normalized transmittance, and the obtained value was $(-2.8 \pm 0.5) \times 10^{-11}$ cm^2/W (corresponding to -8.8×10^{-8} esu). The shape of the open-aperture scan (Figure 8) indicates the presence of reverse saturable absorption (RSA), and the nonlinear absorption coefficient changed from $(4.0 \pm 1.0) \times 10^{-7}$ cm/W at 620 nm to $(12.0 \pm 1.0) \times 10^{-7}$ cm/W at 500 nm. The two-photon absorption contribution to the optical nonlinearity was negligible, and it can be assumed that optical nonlinearity mainly comes from the nonlinear refraction. The *Z*-scan measurements made on PbS nanocrystals doped polymer films[28,29] showed negative nonlinear refractive indexes with absolute values 1 order of magnitude smaller than those measured in our nanocomposite films, while both saturation absorption and two-photon absorption were observed. These differences can be ascribed to different testing parameters and/or different material structure.

(26) Sheik-Bahae, M.; Said, A. A.; Wei, T.-H.; Hagan, D. J.; Van Stryland, E. W. *IEEE J. Quantum Electron.* **1990**, *26*, 760.
(27) Ganeev, R. A.; Ryasnyansky, A. I.; Tugushev, R. I.; Usmanov, T. *J. Opt. A: Pure Appl. Opt.* **2003**, *5*, 409.
(28) Yu, B.; Yin, G.; Zhu, C.; Gan, F. *Opt. Mater.* **1998**, *11*, 17.
(29) Liu, B.; Li, H.; Chew, C. H.; Que, W.; Lam, Y. L.; Kam, C. H.; Gan, L. M.; Xu, G. Q. *Mater. Lett.* **2001**, *51*, 461.

Conclusions

A silica mesostructured thin film was synthesized via evaporation induced self-assembly and doped with PbS nanoparticles via a two-step impregnation. The impregnation process was carried out at room temperature, and under these conditions the matrix retained its original structure as pointed out from SAXS measurements. SIMS together with TEM analyses demonstrated that the diffusion of the PbS precursor solutions was complete and homogeneous in the whole film thickness. PbS nanocrystals growth took place inside the dimensionally controlled mesopores, whose walls prevented their aggregation in bigger clusters during their growth. PbS nanoparticles showed a quantum confinement effect, demonstrated by a clear blue shift of the optical absorption edge with respect to the bulk PbS. The films showed high third-order optical nonlinearity, opening perspectives for this material utilization in optical devices requiring small band gap semiconductors ranging from the visible range to the NIR spectrum.

Acknowledgment. This work has been supported by MURST-FIRB 2001 (RBNE01P4JF) and PRIN 2004.

CM050850J